DOI: 10.1021/cg101125m

CRYSTAL GROWTH & DESIGN Article

2011, Vol. 11
436–444

Three Novel Inorganic−Organic Hybrid Arsenomolybdate Architectures Constructed from Monocapped Trivacant $[As^{III}As^{V}Mo_9O_{34}]^{6-}$ Fragments with $[Cu(L)_2]^{2+}$ Linkers: From Dimer to Two-Dimensional Framework

Qiuxia Han,[†,‡] Pengtao Ma,[†] Junwei Zhao,[†] Ziliang Wang,[†] Wenhua Yang,[†] Penghu Guo,[†] Jingping Wang,*[,†] and Jingyang Niu*[,†]

[†]*Institute of Molecular and Crystal Engineering, School of Chemistry and Chemical Engineering, Henan University, Kaifeng, 475004, P. R. China, and* [‡]*Basic Experimental Teaching Center, Henan University, Kaifeng 475004, P. R. China*

Received August 26, 2010; Revised Manuscript Received November 22, 2010

ABSTRACT: Three novel inorganic−organic hybrid arsenomolybdates constructed from monocapped trivacant $[As^{III}As^{V}Mo_9O_{34}]^{6-}$ fragments with $[Cu(en)_2]^{2+}$ or $[Cu(dap)_2]^{2+}$ linkers, $[Cu(en)_2H_2O]_2\{[Cu(en)_2][Cu(en)_2As^{III}As^{V}Mo_9O_{34}]\}_2\cdot 4H_2O$ (**1**), $(H_2en)_{1.5}[Cu(en)(Hen)][As^{III}As^{V}Mo_9O_{34}]\cdot 2H_2O$ (**2**) (en = ethylenediamine), and $[Cu(dap)_2]_4[Cu(dap)_2(H_2O)][Cu(dap)_2(As^{III}As^{V}Mo_9O_{34})_2]\cdot 2H_2O$ (**3**) (dap = 1,2-diaminopropane), have been successfully synthesized under hydrothermal conditions and structurally characterized by elemental analyses, IR spectra, single-crystal X-ray diffraction, and thermogravimetric (TG) analysis. Single-crystal structural analyses indicate that **1**−**3** all contain the peculiar monocapped trivacant $[As^{III}As^{V}Mo_9O_{34}]^{6-}$ subunit derived from the infrequent trivacant Keggin $[A\text{-}\alpha\text{-}As^{V}Mo_9O_{34}]^{9-}$ fragment with a capping $\{AsO_3\}$ group. Notably, **1**−**3** represent rare inorganic−organic hybrid heteropolymolybdate (HPM) containing $[As^{III}As^{V}Mo_9O_{34}]^{6-}$ subunits, which display the assembly from a zero-dimensional sandwich-type dimer, one-dimensional chain, to a two-dimensional layer by the $[Cu(en)_2]^{2+}$ or $[Cu(dap)_2]^{2+}$ linkers. Surface photovoltage spectroscopy (SPS) and electric field induced surface photovoltage spectroscopy (EFISPS) measurements for **1**−**3** indicate that only **3** has the n-type semiconductor characteristic.

Introduction

Polyoxometalates (POMs), dominated mainly by heteropolytungstate (HPT) and heteropolymolybdate (HPM), with their versatile structural topologies, nucleophilic oxygen-enriched surface, and physicochemical properties in redox, photo, and magnetic chemistry, represent one of the excellent candidates for the development of cluster architectures based on the building-block strategy.[1,2] Recently, considerable attention has been concentrated on highly charged trivacant species, which are able to act as surface oxygen-enriched bulky polydentate ligands incorporation of multiple transition-metal ions and lead to a growing family of transition-metal substituted polytungstates (TMSPs) with various stoichiometries and structural features combined with interesting catalytic, medicinal, and magnetic properties.[3−5] Therefore, large numbers of TMSPs have been developed since the first sandwich-type $[Co_4(H_2O)_2(\alpha\text{-B-}PW_9O_{34})_2]^{10-}$ was found in 1973.[6] Polytungstoarsenates, as one of the most important subfamilies in POMs chemistry, have been extensively reported for structural diversities for several years, most of which are constructed by trivacant Keggin building fragments, such as sandwich-type ($[Cu_3(H_2O)_2(\alpha\text{-}AsW_9O_{33})_2]^{12-}$),[7] $[Cs_2Na(H_2O)_8Pd_3(\alpha\text{-}AsW_9O_{33})_2]^{9-}$,[8] $[M_3(H_2O)_3(\alpha\text{-}AsW_9O_{33})_2]^{12-}$ (M = Mn^{2+}, Co^{2+}, Ni^{2+}, Cu^{2+}, Zn^{2+}) and $[(VO)_3(\alpha\text{-}AsW_9O_{33})_2]^{11-}$,[9] $[M_4(H_2O)_{10}(\beta\text{-}AsW_9O_{33})_2]^{6-}$ (M = Fe^{3+}, Cr^{3+}),[10] $[Cu_4K_2(H_2O)_8(\alpha\text{-}AsW_9O_{33})_2]^{8-}$,[11] banana-shaped clusters $[Ni_6As_3W_{24}O_{94}(H_2O)_2]^{17-}$,[12] $[M_6(H_2O)_2(AsW_9O_{34})_2(AsW_6O_{26})]^{17-}$ (M = Mn^{2+}, Co^{2+}, Zn^{2+}),[13] together with some giant clusters $[As_{12}Ce_{16}(H_2O)_{36}W_{148}O_{524}]^{76-}$,[14] $[As^{III}{}_6W_{65}O_{217}(H_2O)_7]^{26-}$,[15] $[K\subset\{Eu(H_2O)_2(\alpha\text{-}AsW_9O_{33})\}_6]^{35-}$, $[Cs\subset\{Eu(H_2O)_2(\alpha\text{-}AsW_9O_{33})\}_4]^{23-}$,[16] and $[Na(H_2O)_3]_2[Ni(H_2O)_6]_2[Ni(H_2O)_5]\{[Ni_3(dap)(H_2O)_2]_2(H_2W_4O_{16})\}\{(\alpha\text{-}H_2As^{V}W_6O_{26})[Ni_6(OH)_2(H_2O)(dap)_2](B\text{-}\alpha\text{-}HAs^{V}W_9O_{34})\}_2\cdot 7H_2O$.[17]

Compared with abundant heteropolytungstates in TMSP chemistry, the heteropolymolybdate (HPM) analogues are very limited. In particular, investigations on TM-substituted HPMs containing lacunary POM building units are almost laggardly. Presently, the most useful synthetic methods to prepare these HPMs are as follows: (i) by the self-assembly reaction of simple raw materials, and (ii) by the reaction of polymolybdate precursors. Up to now, only a few such examples have been reported. For instance, in 1981, Fukushima et al. reported the first trivacant Keggin sandwich-type HPM $[Cu_2(SiMo_9O_{33})_2]^{12-}$ established by two trivacant $[SiMo_9O_{33}]^{8-}$ units.[18] Until 1996, Müller et al. communicated three trivacant Keggin HPMs $[(AsOH)_3(MoO_3)_3(AsMo_9O_{33})]^{7-}$, $[(AsOH)_6(MoO_3)_2(O_2MoOMoO_2)_2(AsMo_9O_{33})_2]^{10-}$, and $[(AsOH)_4(AsO)_2(HOAs\text{-}O\text{-}MoO_2)_2(O_2Mo{-}O{-}MoO_2)_2(AsMo_9O_{33})_2]^{8-}$.[19] In 2003, May et al. addressed a class of monolanthanide substituted phosphomolybdates $[Ln(PMo_{11}O_{39})_2]^{11-}$ (Ln = Ce^{III}, Sm^{III}, Dy^{III}, Lu^{III}).[20] In 2007 and 2008, Xu and co-workers synthesized two one-dimensional (1-D) di-TM sandwiched arsenomolybdates $[M(H_2O)_5]_{2n}(H_3O)_{2n}\{M(H_2O)_5\}_2(MAs^{V}Mo_9O_{33})_2]_n[M(H_2O)_4(MAs^{V}Mo_9O_{33})_2]^{8n-}$ (M = Mn^{2+}, Co^{2+}) and an isolated di-Mn substituted arsenomolybdate $[Mn_2(As^{V}Mo_9O_{33})_2]^{10-}$, which are all constructed from $[B\text{-}\beta\text{-}As^{V}Mo_9O_{33}]^{7-}$ fragments.[21] Recently, Xue et al.

*To whom correspondence should be addressed. E-mail: jpwang@henu.edu.cn (J.W.) and jyniu@henu.edu.cn (J.N.). Tel: (+86)-378-2886876. Fax: (+86)-378-2886876.

Published on Web 01/07/2011

addressed a series of iso- or hetero-TM sandwiched arsenomolybdates $[M_2(AsMo_7O_{27})_2]^{n-}$ (M = Cr^{III}, n = 12; M = Cu^{II}, n = 14) and $[CrFe(AsMo_7O_{27})_2]^{12-}$ based on the new pentavacant $[As^{III}Mo_7O_{27}]^{9-}$ building blocks using $(NH_4)_6Mo_7O_{24}\cdot 4H_2O$ precursors.[22,23] In 2009, two types of rare sandwich-type germanomalybdates $[M_2(\beta\text{-Y-}GeMo_9O_{33})_2]^{12-}$ (M = Cu^{II}, Cr^{III}) and $[M_4(H_2O)_2(\alpha\text{-B-}GeMo_9O_{34})_2]^{12-}$ (M = Ni^{II}, Mn^{II}, Co^{II}) were prepared by our lab.[24] As illustrated above, reports on TM-substituted arsenomolybdates containing lacunary POM fragments are rather rare, and most of them are purely inorganic and synthesized in conventional aqueous solution, which provides us a large opportunity. As a result, recently, we have launched explorations on the {As−O−Mo} system with the aim of exploring novel inorganic−organic hybrid HPMs based on the following reasons: (1) owing to the lability and instability in the structure of HPMs, it is very difficult to prepare and isolate lacunary HPM precursors; thus, the types and numbers of lacunary HPM precursors are very limited, so we select $Na_2MoO_4\cdot 2H_2O$ as the starting material; (2) the As^{III} element is easy to be oxidized to the As^V element,[25] and moreover, they often employ different coordination geometries (tetrahedron for the As^V element, triangular pyramid for the As^{III} element) incorporating into the polyoxomolybdate backbones in the form of the $[As^VMo_9O_{34}]^{9-}$ or $[As^{III}Mo_9O_{33}]^{9-}$ fragments as the central heteroatoms. Furthermore, the As^{III} atom can cap the surface of the polyoxomolybdate backbones generating $\{AsO_3\}$ capped polyoxomolybdate species. Therefore, As_2O_3 was utilized here; (3) in order to obtain inorganic−organic hybrid HPMs, organoamines were introduced to our system. In this context, we began to exploit the {Cu/As/Mo} system in the presence of ethylenediamine (en) or 1,2-diaminopropane (dap) by hydrothermal technology. Finally, we have successfully obtained three novel inorganic−organic hybrid arsenomolybdates $[Cu(en)_2H_2O]_2\{[Cu(en)_2][Cu(en)_2As^{III}As^VMo_9O_{34}]\}_2\cdot 4H_2O$ (**1**), $(H_2en)_{1.5}[Cu(en)(Hen)][As^{III}As^VMo_9O_{34}]\cdot 2H_2O$ (**2**), and $[Cu(dap)_2]_4[Cu(dap)_2(H_2O)][Cu(dap)_2(As^{III}As^VMo_9O_{34})_2]\cdot 2H_2O$ (**3**). The common feature is that **1**−**3** all contain the peculiar monocapped trivacant $[As^{III}As^VMo_9O_{34}]^{6-}$ subunit derived from the trivacant Keggin $[A\text{-}\alpha\text{-}As^VMo_9O_{34}]^{9-}$ fragment with a capping $\{AsO_3\}$ group. By the $[Cu(en)_2]^{2+}$ or $[Cu(dap)_2]^{2+}$ linkers, **1**−**3** display the assembly from zero-dimensional (0-D) sandwich-type dimer, 1-D chain to two-dimensional (2-D) layer. To the best of our knowledge, **1**−**3** represent the rare inorganic−organic hybrid HPMs containing $[As^{III}As^VMo_9O_{34}]^{6-}$ subunits. More interestingly, the $[As^VMo_9O_{34}]^{9-}$ fragment in the $[As^{III}As^VMo_9O_{34}]^{6-}$ subunit maintains the infrequent A-α-type configuration. In addition, the successful syntheses of **1**−**3** show that hydrothermal techniques offer an effective way for making novel inorganic−organic hybrid HPMs containing trivacant Keggin polyoxoanions, which paves an avenue for the design and syntheses of novel multidimensional HPMs frameworks constructed from trivacant Keggin-type HPMs building units.

Experimental Section

Materials and Methods. All reagents were used as purchased without further purification. Elemental analyses (C, H, and N) were performed using a a Perkin-Elmer 2400 Elemental analyzer. Inductively coupled plasma (ICP) analysis was performed on a Jarrel-Ash J-A1100 spectrometer. IR spectra were obtained from a solid sample pelletized with KBr on Nicolet 170 SXFT-IR spectrometer in the range 400−4000 cm^{-1}. Thermogravimetric analyses were performed on a Perkin-Elmer-7 instrument under nitrogen flow with a heating rate of 10 °C/min in the temperature region of 25−600 °C. Surface photovoltage spectroscopy (SPS) and electric field induced surface photovoltage spectroscopy (EFISPS) were carried out on a lock-in based surface photovoltage measurement system which consisted of a source of monochromatic light, a lock-in amplifier (SR830-DSP) with a light chopper (SR540), a sample cell, and a computer. A low chopping frequency of ~46 Hz was used.

Synthesis. The hydrothermal syntheses were carried out in Teflon-lined reactor under autogenous pressure. The 20 mL vessel was filled by the mixture containing $Na_2MoO_4\cdot 2H_2O$ (0.50 g, 2.0 mmol), As_2O_3 (0.12 g, 0.6 mmol), $CuCl_2\cdot 2H_2O$ (0.21 g, 1.2 mmol), en or dap (0.1 mL), and water (8 mL). All reactants were stirred briefly before heating, and their pH values were adjusted with 1 M HCl. The mixture was heated to 130 °C over a period of five days and naturally cooled to room temperature. The products were isolated by filtration and washed with water. All the chemical reagents were reagent grade and used as commercially purchased without further purification.

Synthesis of $[Cu(en)_2H_2O]_2\{[Cu(en)_2][Cu(en)_2As^{III}As^VMo_9O_{34}]\}_2\cdot 4H_2O$ (1). A mixture of $Na_2MoO_4\cdot 2H_2O$ (0.50 g, 2.0 mmol), As_2O_3 (0.12 g, 0.6 mmol), $CuCl_2\cdot 2H_2O$ (0.21 g, 1.2 mmol), en (0.1 mL), and water (8 mL) was stirred and its pH value was adjusted to 5.4 with 1 M HCl. The resulting suspension was sealed in a 20 mL Teflon-lined reactor and kept at 130 °C for five days. After cooling the autoclave to room temperature, dark blue rod single crystals of **1** were separated, washed with water, and air-dried (34% yield based on Mo element). Elemental analysis (%) calcd $C_{24}H_{108}As_4Cu_6Mo_{18}N_{24}O_{74}$: C, 6.66; N,7.77; H, 2.52; Cu, 8.82; As, 6.93; Mo, 39.93. Found: C, 6.71; N,7.84; H,2.49; Cu, 8.78; As, 6.90; Mo, 39.71. IR (KBr pellet, cm^{-1}): 3432(m), 3302(s), 3254(m), 2939(m), 2885(s), 1585(s), 1458(s), 1397(m), 1276(m), 1165(m), 1099(m), 1041(s), 915(s), 861(s), 755(s), 709 (s), 647(s), 605(m), 535(m), 510(m), 489(m).

Synthesis of $(H_2en)_{1.5}[Cu(en)(Hen)][As^{III}As^VMo_9O_{34}]\cdot 2H_2O$ (2). A mixture of $Na_2MoO_4\cdot 2H_2O$ (0.50 g, 2.0 mmol), As_2O_3 (0.12 g, 0.6 mmol), $CuCl_2\cdot 2H_2O$ (0.21 g, 1.2 mmol), and en (0.1 mL) was dissolved in water (8 mL), stirred, and its pH value was adjusted to 4.6 with 4 M HCl. The resulting suspension was sealed in a 20 mL Teflon-lined reactor and kept at 130 °C for five days. After cooling of the autoclave to room temperature, black green block single crystals of **2** were separated, washed with distilled water, and air-dried in 42% yield based on Mo element. Elemental analysis (%) calcd for $C_7H_{34}As_2CuMo_9N_7O_{36}$: C, 4.50; N, 5.25; H, 1.83; Cu, 3.40; As, 8.02; Mo,46.19. Found: C, 4.54; N, 5.27; H, 1.81; Cu,3.47; As, 7.93; Mo, 45.96. IR (KBr pellet, cm^{-1}): 3439 (m), 3341(s), 3280(s), 3210 (m), 3089(m), 3031(m), 1600(s), 1503(s), 1472(m), 1338(m), 1138(m), 1076(m), 1039(s), 1011(m), 957(m), 931(s), 868(s), 844(s), 782(m), 756(m), 737(m), 644(s), 491 (m).

Synthesis of $[Cu(dap)_2]_4[Cu(dap)_2(H_2O)][Cu(dap)_2(As^{III}As^VMo_9O_{34})_2]\cdot 2H_2O$ (3). A mixture of $Na_2MoO_4\cdot 2H_2O$ (0.50 g, 2.0 mmol), As_2O_3 (0.12 g, 0.6 mmol), $CuCl_2$ $2H_2O$ (0.21 g, 1.2 mmol), dap (0.1 mL), and water (8 mL) was stirred and its pH value was adjusted to 6.4 with 1 M HCl. The resulting suspension was sealed in a 20 mL Teflon-lined reactor and kept at 130 °C for five days. After cooling of the autoclave to room temperature, dark blue block single crystals of **3** were separated, washed with distilled water, and air-dried in 30% yield based on Mo element. Elemental analysis (%) calcd for $C_{36}H_{126}As_4Cu_6Mo_{18}N_{24}O_{71}$: C, 9.74; N, 7.57; H, 2.86; Cu, 8.59; As, 6.75; Mo, 38.90. Found: C, 9.79; N, 7.63; H, 2.76; Cu, 8.50; As, 6.71; Mo, 38.69. IR (KBr pellet, cm^{-1}): 3448(m), 3323(s), 3288(s), 2966(m), 1587(s), 1458(m), 1395(m), 1168(m), 1066(m), 1021(m), 920(s), 903(s), 860(s), 840(s), 755(s), 649(s), 487(m).

X-ray Crystallography. A crystal with dimensions 0.37 × 0.14 × 0.11 mm^3 for **1**, 0.32 × 0.26 × 0.21 mm^3 for **2**, and 0.17 × 0.13 × 0.09 mm^3 for **3** was stuck on a glass fiber and intensity data were collected at 296(2) K on a Bruker Smart APEX II CCD diffractometer with graphite-monochromated Mo−Kα radiation (λ = 0.71073 Å). Routine Lorentz polarization and Multiscan absorption correction were applied to intensity data. Their structures were determined and the heavy atoms were found by direct methods using the SHELXTL-97 program package.[26] The remaining atoms were found from

Table 1. Crystallographic Data Structure Refinement for Compounds 1−3

	1	2	3
empirical formula	$C_{24}H_{108}As_4Cu_6Mo_{18}N_{24}O_{74}$	$C_7H_{34}As_2CuMo_9N_7O_{36}$	$C_{36}H_{126}As_4Cu_6Mo_{18}N_{24}O_{71}$
M, g mol^{-1}	4325.18	1869.25	4439.45
cryst syst	triclinic	monoclinic	monoclinic
space group	$P\bar{1}$	$P2(1)/c$	$P2(1)/c$
a, Å	13.4957(7)	18.847(3)	22.680(3)
b, Å	13.8760(7)	10.0522(16)	21.962(3)
c, Å	13.9977(7)	21.042(3)	24.579(3)
α, deg	96.6240(10)	90	90
β, deg	95.6950(10)	94.180(2)	92.244(2)
γ, deg	94.5110(10)	90	90
V, Å^3	2580.2(2)	3976.0(11)	12233(3)
Z	1	4	4
T, K	296(2)	296(2)	296(2)
d_{calcd}, g cm^{-3}	2.784	3.123	2.410
μ, mm^{-1}	4.697	5.033	3.964
total reflns	13349	19478	61581
indep reflns	8997	7050	21446
parameters	676	559	1332
limiting indices	$-14 \le h \le 16$	$-22 \le h \le 18$	$-26 \le h \le 26$
	$-13 \le k \le 16$	$-11 \le k \le 11$	$-19 \le k \le 26$
	$-16 \le l \le 16$	$-25 \le l \le 23$	$-27 \le l \le 29$
GOF	1.017	1.062	1.018
R_1[a] ($I > 2\sigma(I)$)	0.0438	0.0320	0.0532
wR_2[b] ($I > 2\sigma(I)$)	0.1033	0.0794	0.1151
R_1[a] (all data)	0.0550	0.0350	0.1389
wR_2[b] (all data)	0.1101	0.0810	0.1440
diff peak and hole, e Å^{-3}	3.006, −1.251	1.054, −1.403	1.535, −1.193

[a] $R_1 = \sum||F_o| - |F_c||/\sum|F_o|$. [b] $wR_2 = [\sum w(F_o^2 - F_c^2)^2/\sum w(F_o^2)^2]^{1/2}$; $w = 1/[\sigma^2(F_o^2) + (xP)^2 + yP]$, $P = (F_o^2 + 2F_c^2)/3$, where $x = 0.0444$, $y = 22.1609$ for **1**, $x = 0.0304$, $y = 15.2520$ for **2**, $x = 0.0546$, $y = 0$ for **3**.

successive full-matrix least-squares refinements on F^2 and Fourier syntheses. No hydrogen atoms associated with water molecules were located from the difference Fourier maps. Positions of the hydrogen atoms attached to carbon and nitrogen atoms were geometrically placed. All hydrogen atoms were refined isotropically as a riding mode using the default SHELXTL parameters. For **1**, of 13 349 reflections, 8997 unique reflections ($R_{int} = 0.0244$) were considered observed [$I > 2\sigma(I)$]. The final cycle of refinement including atomic coordinates and the anisotropic thermal parameters converged to $R_1 = 0.0438$ and $wR_2 = 0.1033$ [$I > 2\sigma(I)$]. For **2**, of 19478 reflections, 7050 unique reflections ($R_{int} = 0.0385$) were considered observed [$I > 2\sigma(I)$]. The final cycle of refinement including atomic coordinates and the anisotropic thermal parameters converged to $R_1 = 0.0320$ and $wR_2 = 0.0794$ [$I > 2\sigma(I)$]. For **3**, of 61 581 reflections, 21 446 unique reflections ($R_{int} = 0.0917$) were considered observed [$I > 2\sigma(I)$]. The final cycle of refinement including atomic coordinates and the anisotropic thermal parameters converged to $R_1 = 0.0533$ and $wR_2 = 0.1169$ [$I > 2\sigma(I)$]. Crystallographic data for **1**−**3** are summarized in Table 1.

Results and Discussion

Synthesis. The reactivity of the reaction system including $Na_2MoO_4 \cdot 2H_2O$, As_2O_3, and $CuCl_2 \cdot 2H_2O$ with almost equally stoichiometry in the presence of en or dap under hydrothermal conditions has been investigated, leading to three novel inorganic−organic hybrid arsenatomolybdates $[Cu(en)_2H_2O]_2\{[Cu(en)_2][(Cu(en)_2\ As^{III}As^{V}Mo_9O_{34})]\}_2 \cdot 4H_2O$ (**1**), $(H_2en)_{1.5}[Cu(en)(Hen)][As^{III}As^{V}Mo_9O_{34}] \cdot 2H_2O$ (**2**), and $[Cu(dap)_2]_4[Cu(dap)_2(H_2O)][Cu(dap)_2(As^{III}As^{V}Mo_9O_{34})_2] \cdot 2H_2O$ (**3**). Although **1**−**3** are all prepared with similar conditions and contain the same monocapped trivacant $[As^{III}As^{V}Mo_9O_{34}]^{6-}$ fragments, they display different structural configurations.

As we know, many factors such as pH value, reaction temperature, the selection of reactant, metal ions, organic ligands, stoichiometry, the stability of polyoxoanion, etc. can influence the species and configurations of products. At the beginning, **1** was prepared with the pH value of 5.4. When the pH value was decreased to 4.6, 1-D chain-like **2** was obtained, whereas when the pH value was increased to 5.7, another new 2-D inorganic−organic hybrid dicapped Anderson-type arsenatomolybdate $[Cu(en)_2]_2[(CuO_6)\ Mo_6O_{18}(As_3O_3)_2]$ (**4**) was prepared.[27] Parallel experiments reveal that the pH value of the {Cu/As/Mo} system varying in the range 5.0−5.5 favors the formation of **1**; the lower pH of 4.5−5.0 trends to the formation of **2**, whereas the higher pH of 5.5−7.0 favors the preparation of **4**. Possibly, the higher pH value does not favor the stability of the $[As^{III}As^{V}Mo_9O_{34}]^{6-}$ fragment and is prone to the formation of the dicapped Anderson-type $[(CuO_6)Mo_6O_{18}(As_3O_3)_2]^{4-}$ polyoxoanion. Therefore, the pH value plays an important role in the formation and crystallization of **1**−**4**. Besides, when dap was used to replace en in the preparation of **1** or **2**, 2-D layer-like **3** was obtained in the pH value range of 5.0−7.0. Thus, the different organic ligands have a great influence on the construction of multidimensional structural frameworks in our case. Similar phenomena are very common in the {TM//W} reaction system.[28] According to the literature,[22,29] when the starting reactant $Na_2MoO_4 \cdot 2H_2O$ was replaced by $(NH_4)_6Mo_7O_{24} \cdot 4H_2O$ in the synthesis of **3** within the pH range of 6.0−7.0, an unusual 6^3 topology honeycomb network $[Cu(enMe)_2]_3[As_3Mo_3O_{15}]_2 \cdot 2H_2O$ was obtained. When dap was replaced by imidazole (imi) or acetate (OAc), another two new arsenatomolybdates $(As_6CuMo_6O_{30})\{[Cu(imi)_4]_3[As_6CuMo_6O_{30}]\}_2 \cdot 6H_2O$ and $(NH_4)_{10}\{Cu(H_2O)_4\}[AsMo_6O_{21}(OAc)_3]_2 \cdot 12H_2O$ were obtained.[29] In the absence of organic ligands, a novel sandwich-type polyoxoanion $[As_2Cu_2Mo_{14}O_{54}]^{14-}$ can be obtained.[22] Thus, it can be seen that selection of Mo-containing materials and organic ligands are of importance in designing and assembling expected HPMs. In summary, Mo-containing materials, pH and organic ligands have a great influence on the structural diversity of the product phases. Therefore, the systematic exploration of the {TM/As/Mo} system still remains a great challenge to us.

Scheme 1. The Formation Conditions of the Relative Arsenatomolybdates

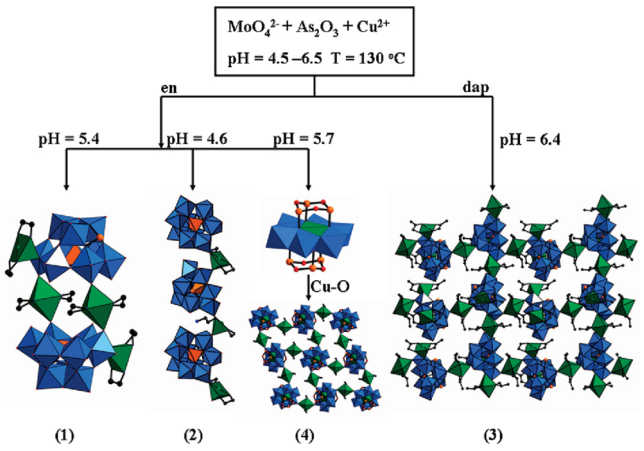

The continuous work is in progress. Scheme 1 illustrates the formation conditions of the related arsenatomolybdates.

Crystal Structures. Compounds **1**−**3** were all prepared by exploitation of the reaction of $Na_2MoO_4 \cdot 2H_2O$, As_2O_3, and $CuCl_2 \cdot 2H_2O$ in the presence of organoamines under hydrothermal conditions. The common and striking feature of **1**−**3** is that they all contain the same monocapped trivacant Keggin $[As^{III}As^{V}Mo_9O_{34}]^{6-}$ unit, although dimeric, 1-D chain-like, and 2-D layer-like assemblies are used by them, respectively. The $[As^{III}As^{V}Mo_9O_{34}]^{6-}$ unit is derived from the trivacant Keggin $[As\text{-}\alpha\text{-}As^{V}Mo_9O_{34}]^{9-}$ moiety, which is capped by a triangular pyramidal $\{AsO_3\}$ group. In the skeleton, the tetrahedral $\{AsO_4\}$ group resides in the central of the $[As\text{-}\alpha\text{-}As^{V}Mo_9O_{34}]^{9-}$ Keggin cluster and shares four oxygen atoms with a $\{Mo_3O_{13}\}$ triad and three $\{Mo_2O_{10}\}$ groups, whereas the $\{AsO_3\}$ group caps the square window of the trivacant $[As\text{-}\alpha\text{-}As^{V}Mo_9O_{34}]^{9-}$ Keggin fragment surrounded by a $\{Mo_3O_{13}\}$ triad and a $\{Mo_2O_{10}\}$ group. Bond valence sum (BVS)[30] calculations for all the As atoms in **1**−**3** illustrate that the oxidation states of four-coordinate As and three-coordinate As elements are +5 and +3, respectively. These results are in good agreement with their usual geometric configurations. Notably, only As_2O_3 was used as the starting material; however, the As^{V} element was observed in the products. Therefore, part of As_2O_3 reactants must have been oxidized in the reaction. Similar phenomenon can be observed in previous literature reports.[25] Although the monocapped trivacant $[As^{III}As^{V}Mo_9O_{34}]^{6-}$ isomer derived from the trivacant Keggin $[A\text{-}\beta\text{-}As^{V}Mo_9O_{34}]^{9-}$ moiety was reported in 1999,[31] obviously different, the $[As^{III}As^{V}Mo_9O_{34}]^{6-}$ unit in **1**−**3** is derived from trivacant Keggin $[A\text{-}\alpha\text{-}As^{V}Mo_9O_{34}]^{9-}$ moiety. To the best of our knowledge, it is very rare that the A-α-type trivacant Keggin fragment is maintained in the solid structure.

Single-crystal X-ray diffraction reveals that **1** consists of two $\{[Cu(en)_2][(As^{III}As^{V}Mo_9O_{34})]\}^{4-}$ units linked by two $[Cu(en)_2]^{2+}$ cations leading to a unusual sandwich-type dimeric polyoxoanion $\{[Cu(en)_2][Cu(en)_2As^{III}As^{V}Mo_9O_{34}]\}_2^{2-}$, two discrete $[Cu(en)_2H_2O]^{2+}$ cations, and four lattice water molecules. The sandwich-type polyoxoanion (Figure 1) is constructed from two crystallographically symmetric $\{[Cu(en)_2][(As^{III}As^{V}Mo_9O_{34})]\}^{4-}$ units and two $[Cu(en)_2]^{2+}$ complex cations via two O−Cu−O bridges. The $\{[Cu(en)_2][(As^{III}As^{V}Mo_9O_{34})]\}^{4-}$ unit is derived from the trivacant Keggin $[A\text{-}\alpha\text{-}As^{V}Mo_9O_{34}]^{9-}$ moiety, which is capped by a triangular pyramidal $\{AsO_3\}$ group and attaches a $[Cu(en)_2]^{2+}$ complex cation to a bridging oxygen atom (O27). It is noteworthy that the sandwich-type $\{[Cu(en)_2][Cu(en)_2As^{III}As^{V}Mo_9O_{34}]\}_2^{2-}$ polyoxoanion constructed by two $[A\text{-}\alpha\text{-}As^{V}Mo_9O_{34}]^{9-}$ moieties has been first observed.

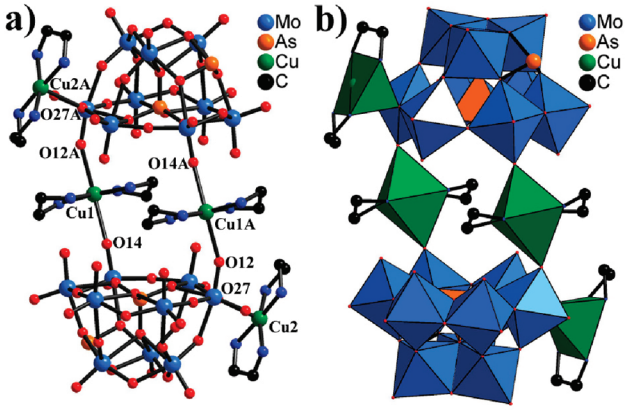

Figure 1. (a) Ball-and-stick and (b) combined polyhedral/ball-and-stick representation of dimeric sandwich-type polyoxoanion in **1** with selected labeling scheme. The atoms with "A" in their labels are symmetrically generated (A: $0.5 - x$, $0.5 - y$, $-z$). Hydrogen atoms were omitted for clarity.

Three crystallographically unique Cu^{2+} cations in **1** display different coordinated configurations. The six-coordinate Cu1 atom resides in the distorted octahedral geometry, which is defined by four N atoms from two en ligands [Cu1−N: 1.999(7)−2.010(8) Å] building the equatorial plane, O14 and O12A ($-x$, $1 - y$, $-z$) atoms from two adjacent $[As^{III}As^{V}Mo_9O_{34}]^{6-}$ units [Cu1−O14: 2.508(6) Å, Cu1−O12A: 2.517(7) Å] lying on the polar sites of the elongated octahedron. The five-coordinate Cu2 atom grafts on the two trivacant $[As^{III}As^{V}Mo_9O_{34}]^{6-}$ units via a bridging oxygen atom (O27) and adopts square-pyramid geometry, which is coordinated by four N atoms from two en molecules [Cu2−N: 1.991(7)−2.003(7) Å] building a basal plane and one O27 atom from the $[As^{III}As^{V}Mo_9O_{34}]^{6-}$ unit [Cu1−O27: 2.499(6) Å] occupying the apical position. The Cu3 complex cation acts as a discrete counteraction, which also displays square-pyramid architecture. The Cu3 center is covalently bonded to four N donors from two en molecules [Cu3−N: 1.985(8)−2.018(8) Å] and one water ligand [Cu3−O1W: 2.418(7) Å].

In the polyoxoanion of **1**, two monocapped trivacant $[As^{III}As^{V}Mo_9O_{34}]^{6-}$ subunits are combined together by $[Cu1(en)_2]^{2+}$ and $[Cu1A(en)_2]^{2+}$ (A: $-x$, $1 - y$, $-z$) complex cations, leading to an abnormal bis(TM-complex) substituted sandwich-type assembly. In addition, several poly(TM-complex) substituted sandwich-type POMs have been reported.[32−39] For example, in 2005, Pope et al. reported a novel mono-$[Co(en)]^{3+}$ complex sandwiched tungstophosphate $[\{Co(en)WO_4\}WO(H_2O)(PW_9O_{34})_2]^{13-}$ (Figure S1a, Suppporting Information).[32] In 2008, our group reported a 1-D chain tungstoantimonate established by inorganic−organic hybrid tri-Mn sandwiched units $[Mn_3(\mu\text{-}OAc)_2(B\text{-}\alpha\text{-}SbW_9O_{33})_2]^{14-}$ (Figure S1b, Suppporting Information) via one acetate bridge.[33] Synchronously, Yang et al. and Wang et al. respectively reported a series of tetra-Ni^{II} complex sandwiched POMs $[M_4(Hdap)_2(HXW_9O_{34})_2]^{n-}$ (M = Zn or Ni, X = Si, P, Ge) and $[Ni_4(L)_2(PW_9O_{34})_2]^{10-}$ (L = dap or hexamethylene diamine) (Figure S1c, Suppporting

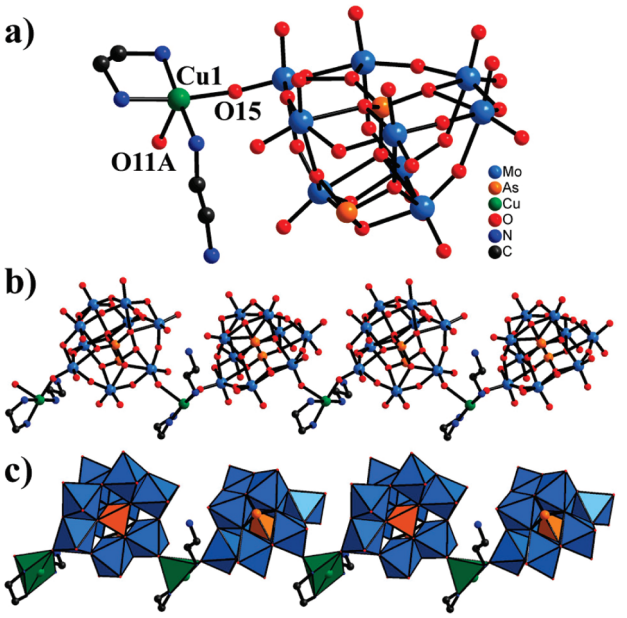

Figure 2. (a) Ball-and-stick representation of polyoxoanion in **2** with selected labeling scheme; (b) Ball-and-stick and (c) combined polyhedral/ball-and-stick representation of the 1-D chain-like arrangement of **2**. The atoms with "A" in their labels are symmetrically generated (A: $x, -1.5 - y, 0.5 + z$).

Information).[34,35] Subsequently, Dolbecq et al. addressed a novel hybrid tetra-Fe^{III} sandwiched tungstoantimonate $[Fe^{III}_4(ox)_4(H_2O)_2\ (SbW_9O_{33})_2]^{14-}$ (Figure S1d, Suppporting Information).[36] In the same year, our group also reported two hexa-Cu-complex sandwiched tungstogermanates $[Cu_6(L)_2(B\text{-}\alpha\text{-}GeW_9O_{34})_2]^{8-}$ (L = 2,2′-bipy, phen) (Figure S1e, Suppporting Information),[37] and Yang's group synthesized another two hybrid hexa-Cu^{II} sandwiched POMs $[Cu_6(dap)_2(B\text{-}\alpha\text{-}SiW_9O_{34})_2]^{8-}$ and $[Cu_6(en)_2(B\text{-}\alpha\text{-}GeW_9O_{34})_2]^{8-}$ (Figure S1f, Suppporting Information).[38] Recently, Yang et al. also described a series of hybrid octa-Cu^{II} cluster substituted sandwich-type POMs $[Cu_8(dap)_4(H_2O)_2(B\text{-}\alpha\text{-}XW_9O_{34})_2]^{4-}$ (X = Si, L = en or dap; X = Ge, L = dap or 2,2′-bpy) (Figure S1g, Suppporting Information) and a dual-organic ligands hybrid mixed-valent octa-Cu sandwiched tungstogermanate $[Cu^{I}_2Cu^{II}_6(2,2'\text{-bpy})_2(4,4'\text{-bpy})_2(B\text{-}\alpha\text{-}GeW_9O_{34})_2]^{14-}$ (Figure S1h, Suppporting Information).[39] As shown above, all of these reported hybrid sandwich-type POMs are polyoxotungstates; however, there is no report on the hybrid sandwich-type HPMs. To our knowledge, **1** not only represents a first TM-complex substituted sandwich-type HPM, but also a new kind of dinuclear TM-sandwiched POM.

Different from **1**, **2** displays the first 1-D chain formed by monocapped trivacant polyoxoanions $[As^{III}As^{V}Mo_9O_{34}]^{6-}$ linked by onefold $[Cu(en)(Hen)]^{3+}$ complex bridges. In the structure of **2** (Figure 2a), only one crystallographically unique Cu^{2+} cation resides in the asymmetrical unit of **2**. The Cu1 atom adopts a five-coordinate square pyramid, in which the basal plane is defined by three N atoms from two en ligand (Cu−N: 1.973(5)−2.012(5) Å) and one terminal O atom (O15) from the lacunae of $[As^{III}As^{V}Mo_9O_{34}]^{6-}$ unit (Cu−O: 1.971(4) Å), and one O atom (O11A, A: $x, -1.5 - y, 0.5 + z$) from the lacunae of another adjacent $[As^{III}As^{V}Mo_9O_{34}]^{6-}$ unit occupies the apical position (Cu−O: 2.359(4) Å). It should be noted that the Cu1 atom bears two en ligands, in which one acts as a bidentate chelate ligand, and the other uses only a terminal N donor coordinating to the Cu1 atom with the noncoordinate N atom being monoprotonated. The larruping coordinate motif is peculiar in the field of POMs chemistry. Now each Cu1 atom bonds to two O atoms from two neighboring $[As^{III}As^{V}Mo_9O_{34}]^{6-}$ polyoxoanion forming a 1-D chain built by alternate $[Cu(en)(Hen)]^{3+}$ cations and $[As^{III}As^{V}Mo_9O_{34}]^{6-}$ units (Figure 2b,c). To date, 1-D chain-like POMs containing lacunary building blocks have been widely reported. For example, in 2006, a 1-D chain-like tungstoantimonate $Na[\{Cu(2,2'\text{-bpy})(H_2O)\}_2\{Cu(2,2'\text{-bpy})\}_2(B\text{-}\alpha\text{-}SbW_9O_{33})]$ with Na^+ bridges and a 1-D chain tungstogermanate $\{[Cu_4(GeW_9O_{34})_2][Cu(en)_2]\}^{10-}$ constituted by sandwich-type $[Cu_4(GeW_9O_{34})_2]^{12-}$ subunits linked by octahedral $[Cu(en)_2]^{2+}$ bridges were communicated by our group.[40] In comparison with those reported 1-D chains, the five-coordinate square pyramidal $[Cu(en)(Hen)]^{3+}$ linker in **2** was first observed. As a result, **2** represents the first one-dimensional chain assembled by monocapped trivacant $[As^{III}As^{V}Mo_9O_{34}]^{6-}$ polyoxoanions.

The novel 2-D framework of **3** is based on a dimeric asymmetric cluster unit $[Cu(dap)_2]_4[Cu(dap)_2(H_2O)][Cu(dap)_2(As^{III}As^{V}Mo_9O_{34})_2]$ (Figure 3a), which is comprised of two crystallographically unique building units $[As^{III}As^{V}Mo_9O_{34}]^{6-}$ linked together by $[Cu3(dap)_2]^{2+}$ bridges forming a dimeric polyoxoanion $[Cu(dap)_2(As^{III}As^{V}Mo_9O_{34})_2]^{8-}$. It should be noted that two $[As^{III}As^{V}Mo_9O_{34}]^{6-}$ moieties in **3** are somewhat different. One is the same as that in **1** or **2**, whereas the other $[As^{III}As^{V}Mo_9O_{34}]^{6-}$ moiety in **3**, a monocapped $\{AsO_3\}$ group, is statistically disordered over two sides with 0.5 probability. Besides the bridging $[Cu3(dap)_2]^{2+}$ complex cation, six $[Cu(dap)_2]^{2+}$ and a $[Cu(dap)_2(H_2O)]^{2+}$ pendants are supported on two $[As^{III}As^{V}Mo_9O_{34}]^{6-}$ moieties of the dimeric polyoxoanion leading to hepta-supporting skeleton. Therefore, the dimeric polyoxoanion can work as a heptadentate ligand to coordinate to $[Cu(dap)_2]^{2+}$ or $[Cu(dap)_2(H_2O)]^{2+}$ complex cations. According to their roles as a bridging or decorating group, these Cu^{2+} cations can be divided into two classes. The bridging groups including Cu1, Cu1A ($x, 0.5 - y, 0.5 + z$), Cu2, Cu2B ($-1 + x, y, z$), and Cu3 cations are all octahedrally coordinated by four equatorial N donors from two en ligands building a basal plane, and two trans-oxo atoms from two neighboring building units lying on two polar sites of the elongated octahedron. As a result of the evident Jahn−Teller distortion of Cu^{2+} ions in the crystal field leading to the elongation of the Cu−O distances, the axial Cu−O bond distances [2.400(5)−2.877(7) Å] are obviously longer than equatorial Cu−N bond distances [1.975(11)−2.017(9) Å]. The decorating Cu^{2+} cations including Cu4, Cu5, and Cu6 atoms reside in two different coordination environments: square-pyramid and octahedral geometries. Cu4 and Cu5 centers all display square-pyramid geometry, which are all combined with four N donors from two en ligands [Cu4−N: 1.972(10)−2.020(9) Å and Cu5−N: 1.964(3)−1.996(3)Å] lying on the equatorial plane, one terminal O atom (O21) and one bridging O atom (O56) occupying the apical position with the Cu4−O distance of 2.4534(4) Å and the Cu5−O distance of 2.2693(4) Å, respectively. Different from the square-pyramid coordinate mode of Cu4 and Cu5 atoms, the Cu6 atom adopts the octahedral geometry, which is defined by four N atoms from two en ligands [Cu6−N: 1.990(8)−2.006(8) Å] building the equatorial plane, O47 atom [Cu6−O47: 2.521(7) Å] and a water ligand O1W [Cu6−O1W: 2.923(11) Å] occupying the axial positions.

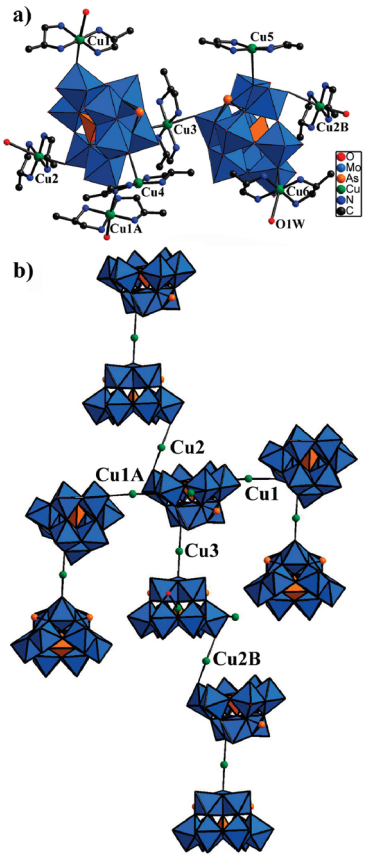

Figure 3. (a) Polyhedral/ball-and-stick representation of the dimeric asymmetric unit $[Cu(dap)_2]_4$ $[Cu(dap)_2(H_2O)][Cu(dap)_2(As^{III}As^{V}Mo_9O_{34})_2]$ in **3**; (b) the connection mode of the dimeric polyoxoanion, dap molecules are omitted for clarity, symmetrical codes: A: x, $0.5 - y$, $0.5 + z$, B: $-1 + x$, y, z.

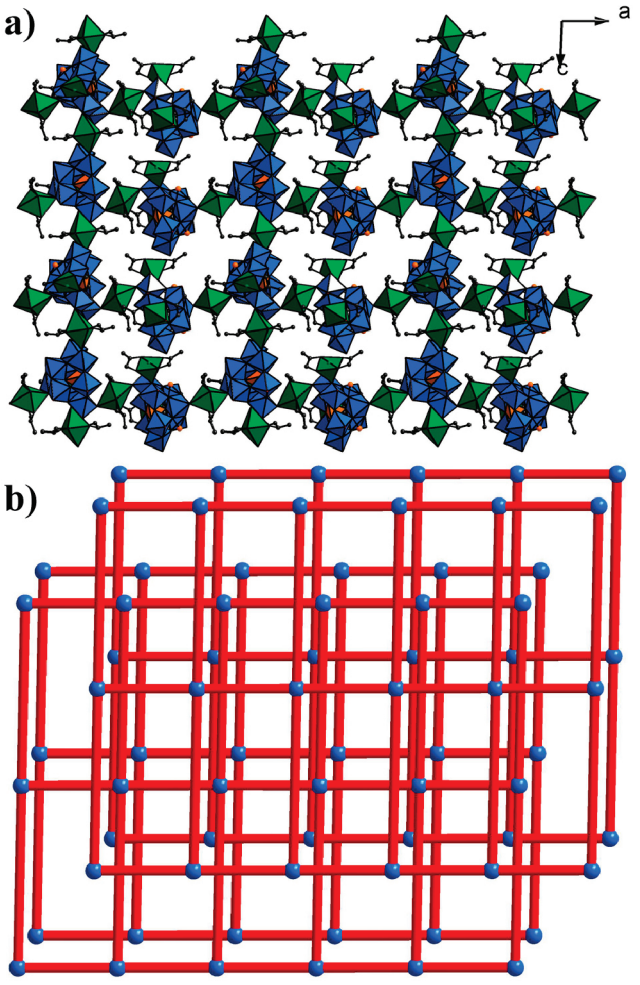

Figure 4. (a) Polyhedral/ball-and-stick representation of 2-D layer-like arrangement of **3** along the *ac* plane; (b) the 2-D grid-like (4, 4) topological network of **3** along the *ac* plane and packing along the *b* axis. Blue balls are the four-connected nodes and represent dimeric polyoxoanion.

In the structure of **3**, the $[Cu3(dap)_2]^{2+}$ bridge links two $[As^{III}As^{V}Mo_9O_{34}]^{6-}$ moieties generating the dimeric polyoxoanion, and another four $[Cu(dap)_2]^{2+}$ bridging groups graft on the surface of the polyoxoanion; thus the polyoxoanions are simultaneously connected with four peripheral polyoxoanions via the four $[Cu(dap)_2]^{2+}$ bridges (Figure 3b). As a result, these polyoxoanions are alternately linked by the linkage of $[Cu1(dap)_2]^{2+}$ bridging cations to form a 1-D chain along the *c* axis with the linkage mode of {−polyoxoanion−$[Cu1(dap)_2]^{2+}$−polyoxoanion−}, and these polyoxoanions are connected with each other through $[Cu2(dap)_2]^{2+}$ bridges resulting in a 1-D chain down the *a* axis with the linkage mode of {−polyoxoanion−$[Cu2(dap)_2]^{2+}$−polyoxoanion−}. Depending on such a crossing linking mode, adjacent polyoxoanions are linked through two types of $[Cu(dap)_2]^{2+}$ linkers into a 2-D layer-like framework along the *ac* plane (Figure 4a). From a topological point of view, if the dimeric polyoxoanion units are viewed as four-connected nodes, the structure displays a grid-like 2-D (4,4)-network topology (Figure 4b). In addition, the layers alternately pack along the *b* axis with the type −A−B−A−B− (Figure 4b).

It should be mentioned that supramolecular architectures attract great interest in the field of supramelocular chemistry and crystal engineering because they can provide novel topology and functional materials. From the viewpoint of supramelocular chemistry, supramolecular architectures are also present in compounds **1**−**3** regarding hydrogen-bonding interactions between nitrogen atoms of organoamine ligands and surface oxygen atoms of polyoxoanions or water molecules. Specifically, N atoms from organoamine ligands act as the proton donors, O atoms from the surface oxygen of $[As^{III}As^{V}Mo_9O_{34}]^{6-}$ units or water molecules serve as the proton acceptors, and then donors and acceptors are hydrogen-bonded together generating the infinitely extended 3-D supramolecular networks (Figures S2−S4, Supporting Information). Within the matrix, abundant N−H···O hydrogen bonds including intra- and intermolecular hydrogen bonds exist between organoamines and the surface oxygen atoms of polyoxoanions or water molecules with N···O distances in the range of 2.909−3.347 Å for **1**, 2.734−3.493 Å for **2**, and 2.826−3.397 Å for **3** (Tables S1−S3, Supporting Information). Moreover, the formation of these supramolecular interactions may be favorable for the chemical stability of **1**−**3**.

In general, three novel inorganic−organic hybrid arsenatomolybdates are successfully obtained and display from dimer, 1-D chain, to 2-D layer architectures constructed from monocapped trivacant $[As^{III}As^{V}Mo_9O_{34}]^{6-}$ fragments with $[Cu(L)_2]^{2+}$ linkers. In the architectures of **1**−**3**, considering the evident Jahn−Teller distortion of Cu^{II} cations in the crystal field leading to the elongation of Cu−O distances,

numerous $[Cu(L)_2]^{2+}$ complex cations are decorated on the surface of $[As^{III}As^{V}Mo_9O_{34}]^{6-}$ fragments. Among them, the $[Cu(L)_2]^{2+}$ linkers play a critical role in the assemblies from dimer, 1-D chain, to 2-D layer. The Cu^{2+} cation shows more flexible coordination geometries (trigonal bipyramid, square pyramid, and octahedron); especially, the Jahn−Teller effect of the octahedra may overcome larger steric hindrance and help to construct extended multidimensional architectures. Actually, this phenomenon was viewed as a "synergistic effect", which was usually used to construct larger aggregates or novel extended frameworks. In this aspect, a lot of work with regard to the combination chemistry of high-nuclear-Cu-substituted POMs driven by the Cu^{II}-polyhedra distortion has been done by Yang's group.[38,39,41] Accordingly, the elongation of Cu−O distances is favorable for the formation and chemical stability of multidimensional POM architectures. Compared with Cu^{2+} cations, lanthanide cations are considered as excellent candidates due to their more coordination requirements and long bond lengths, which in principle can replace Cu^{2+} cations to construct novel multidimensional frameworks. We believe that more interesting results will be obtained in due time. The related work is under progress in our lab.

IR Spectra. The IR spectra of **1**−**3** display the characteristic vibration patterns derived from the Keggin framework in the region of 1100−700 cm^{-1} (Figure S5, Supporting Information). Four characteristic vibration bands attributable to $\nu(As-O_a)$, $\nu(W-O_t)$, $\nu(W-O_b)$, and $\nu(W-O_c)$ appear at 1097−1041, 915, 861, 836−755 cm^{-1} for **1**, 1076−1011, 930, 868 and 844−737 cm^{-1} for **2**, 1066−1021, 905, 860 and 840−755 cm^{-1} for **3**, respectively. In addition, the stretching bands of the −OH and $-NH_2$ groups are observed at 3432 cm^{-1} and 3302−3254 cm^{-1} for **1**, 3439 cm^{-1} and 3341−3280 cm^{-1} for **2**, and 3448 cm^{-1} and 3350−3288 cm^{-1} for **3**, respectively. The bending vibration bands of $-NH_2$ and $-CH_2$ groups appear at 1587−1576 cm^{-1} and 1472−1458 cm^{-1}, respectively. The weak resonances between 1395 and 1165 cm^{-1} are attributed to C−N stretching modes. The occurrence of these resonance signals confirms the presence of organic amine groups, being in good agreement with the single-crystal structural analyses.

Thermogravimetric Analyses. In order to examine the thermal stability, thermogravimetric analyses (TG-DTA) were performed in flowing air atmosphere with a heating rate of 10 °C min^{-1} on the pure samples of **1**−**3**. The TG curve of **1** (Figure S6, Supporting Information) exhibits two steps of weight loss. The first weight loss of 2.51% (cacld. 2.50%) between 25 and 206 °C corresponds to the loss of four lattice water molecules and two structural water molecules. The second weight loss of 22.41% up to 448 °C is assigned to the removal of 12 en ligands and most of the As_2O_3 escaping. In the corresponding DTA curve, the two lesser endothermal peaks at 31 and 242 °C were resulted from the removal of lattice water molecules and sublimation of As_2O_3 groups. Another one evidently a exothermal peak at 440 °C indicated the oxidation of en organic ligands together with the collapse of the polyoxoanion framework, in which 12 en molecules have been lost.

The TG curve (Figure S7, Supporting Information) of **2** is similar to that of **1**; first it gradually loses two lattice water molecules (calc. 1.93%) from 25 to 174 °C, going with one endothermic peak observed at 150 °C in the corresponding DTA curve. On further heating, the materials lose weight continuously during the second step with a combined weight loss of 20.50% from 228 to 450 °C, corresponding to the removal of 1 en, 1 monoprotonented en, 1.5 diprotonted en ligands, and most of the As_2O_3 escaping. In the corresponding DTA curve, one endothermic peak is observed at 255 °C due to the escaping of the As_2O_3 component, and a remarkable exothermal peak at around 439 °C arises from the combustion of en ligands together with the collapse of the polyoxoanion framework.

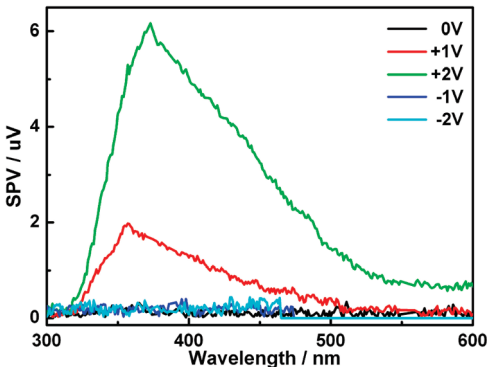

Figure 5. SPS (no external bias) and EFISPS (under external bias different positive and negative electric fields) spectra of **3**.

The TG-DTA curve (Figure S8, Supporting Information) of **3** indicates that the weight loss can be divided into two steps. The first weight loss of 3.84% during the first step from 25 to 120 °C involves the loss of two lattice water molecules and supface rudimental water molecules, going with a wide endothermic peak at around 42 °C on the DTA curve. The second continuous weight loss of 25.02% among 266 to 487 °C is ascribed to the escaping of one molecule of As_2O_3 (calc. 4.46%) and the loss of 12 dap ligands (calc. 20.04%), accompanying a lesser endothermic peak at 294 °C and a remarkable exothermal peak at around 444 °C on the corresponding DTA curve, respectively.

Surface Photovoltage Spectroscopy. The surface photovoltage spectroscopy (SPS) method, acting as an effective tool to investigate the photophysical property of excited states generated by absorption in the aggregate state, is a well-established technique for semiconductor characterization that relies on analyzing illumination-induced changes in the surface voltage,[42] which can reflect photogenerated charge separation and transfer behavior as well as optical absorption characteristics of semiconductor samples, especially for the field-induced surface photovoltage spectroscopy (EFISPS) method, in which the SPS is combined with the electric-field-modified technique.[43] In the present paper, the SPS and EFISPS of **1**−**3** are all performed to investigate the behavior of photogenerated electrons and the photoelectric property under zero field and the external electric fields; nevertheless, only **3** displays markedly SPV response as shown in Figure 5. The SPS and EFISPS of **3** are performed in the range of 300−600 nm with the external electric fields being −2, −1, 0, +1, and +2 V, respectively. When a positive electric field is employed, the SPV response intensity evidently rises with increasing field strength, which is attributed to the same direction of added-outer as built-in field.[44] Furthermore, the SPV response strengthens rapidly with a positive electric field enhancing, which means that more electrons reach the surface owing to the increase of the diffusion length among electrons in the conduction band,[45] whereas when a negative electric field is applied, the SPV response intensity decreases and reduces to invisible, which

results from the electrons in the conduction band moving toward the bulk as a negative electric field is being used.[45] In addition, the band of SPV response disappear entirely once the electric field is evacuated. From Figure 5, it is seen that the sample **3** displays two pronounced SPV response bands in the range of 300−500 nm, which are assigned to band-to-band and exciton transitions, respectively.[46] Besides, it is observed that the bands gradually red shift with an increase in the positive electric fields. The phenomenon can be explained following the Stark effect model;[47] namely, the electrons in bulk on the irradiated side of the electrode move to the surface on the same side of the sample under the inducement of a positive electric field. With an increase in the electric field intensity, the electron density at the top of valence band is enhanced. The addition of state density will increase the probability of excited transition, leading to the red shift phenomenon.[48] Therefore, the behavior that increased positive electric field results in an increase in the SPV response intensity; meanwhile, a decrease in the negative electric fields leads to a decrease in the SPV response intensity, indicating that **3** is the n-type conduction characteristic.[48] A similar phenomenon is also observed in our previous work.[24]

Conclusions

In summary, three novel inorganic−organic hybrid arsenomolybdate architectures constructed from monocapped trivacant $[As^{III}As^{V}Mo_9O_{34}]^{6-}$ fragments with $[Cu(en)_2]^{2+}$ or $[Cu(dap)_2]^{2+}$ linkers have been successfully obtained under hydrothermal conditions. The common feature of **1**−**3** is that they all contain the same monocapped trivacant $[As^{III}As^{V}Mo_9O_{34}]^{6-}$ subunits derived from trivacant Keggin $[A\text{-}\alpha\text{-}As^{V}Mo_9O_{34}]^{9-}$ fragments. **1** represents the first example of unusual inorganic−organic hybrid sandwich-type HPM containing two $[As^{III}As^{V}Mo_9O_{34}]^{6-}$ subunits linked by two discrete $[Cu(en)_2]^{2+}$ cations, **2** represents the first 1-D HPM framework constructed from $[As^{III}As^{V}Mo_9O_{34}]^{6-}$ fragments bridged by $[Cu(en)(Hen)]^{3+}$ linkers, whereas **3** represents an unprecedented 2-D HPM layer-like framework built up from $[As^{III}As^{V}Mo_9O_{34}]^{6-}$ fragments and $[Cu(dap)_2]^{2+}$ linkers. SPS and EFISPS measurements for **1**−**3** indicate that only **3** has the n-type semiconductor characteristic. The successful syntheses of **1**−**3** further testify that the Jahn−Teller effect of Cu^{II} octahedra with axial elongation is an non-negligible driving force, which can provide guidance for discovering novel HPMs containing other lacunary building fragments with a novel topology accompanying unique properties. In addition, lanthanide cations can be taken as good candidates of Cu^{2+} cations combined with lacunary HPM fragments to obtain novel extended POM architectures. Therefore, it is reasonable to believe that the present work will be resposible for expanding the study of HMP-based materials.

Acknowledgment. This work was supported by the Natural Science Foundation of China, Special Research Fund for the Doctor Program of Higher Education, Innovation Scientists and Technicians Troop Construction Projects of Henan Province, the Foundation of Education Department of Henan Province and Natural Science Foundation of Henan Province.

Supporting Information Available: Hydrogen bond tables, hydrogen bonging packing plots, IR spectra, and TG-DTA curves of **1**−**3**. These materials are available free of charge via the Internet at http://pubs.acs.org. CIF files are available online from the Cambridge Crystallographic Data Centre [CCDC nos. 790202−790204 for **1**−**3**].

References

(1) Pope, M. T. *Heteropoly and Isopoly Oxometalates*; Springer: Berlin, 1983.
(2) (a) Pope, M. T.; Müller, A. *Angew. Chem. Int.* **1991**, *30*, 34–38. (b) Long, D.-L.; Burkholder, E.; Cronin, L. *Chem. Soc. Rev.* **2007**, *36*, 105–121.
(3) (a) Müller, A.; Peters, F.; Pope, M. T.; Gatteschi, D. *Chem. Rev.* **1998**, *98*, 239–271. (b) Rhule, J. T.; Hill, C. L.; Judd, D. A.; Schinazi, R. F. *Chem Rev* **1998**, *98*, 327–357.
(4) Clemente-Juan, J. M.; Coronado, E. *Coord. Chem. Rev.* **1999**, *193*−*195*, 361–394.
(5) (a) Bölsing, M.; Nöh, A.; Loose, I.; Krebs, B. *J. Am. Chem. Soc.* **1998**, *120*, 7252–7259. (b) Ben-Daniel, R.; Neumann, R. *Angew. Chem., Int. Ed.* **2003**, *42*, 92–95. (c) Zheng, S.-T.; Yuan, D.-Q.; Jia, H.-P.; Zhang, J.; Yang, G.-Y. *Chem. Commun.* **2007**, 1858–1860.
(6) Weakly, T. J. R.; Evans, H. T.; Showell, J. S.; Tourné, G. F.; Tourné, C. M. *J. Chem. Soc. Chem. Commun.* **1973**, *4*, 139–140.
(7) Robert, F.; Leyrie, M.; Hervé, G. *Acta Crystallogr.* **1982**, *B38*, 358–362.
(8) Bi, L.-H.; Kortz, U.; Keita, B.; Nadjo, L.; Daniels, L. *Eur. J. Inorg. Chem.* **2005**, 3034–3041.
(9) (a) Kortz, U.; Al-Kassem, N. K.; Savelieff, M. G.; Al Kadi, N. A.; Sadakane, M. *Inorg. Chem.* **2001**, *40*, 4742–4749. (b) Mialane, P.; Marrot, J.; Rivière, E.; Nebout, J.; Hervé, G. *Inorg. Chem.* **2001**, *40*, 44–48.
(10) Kortz, U.; Savelieff, M. G.; Bassil, B. S.; Keita, B.; Nadjo, L. *Inorg. Chem.* **2002**, *41*, 783–789.
(11) Kortz, U.; Nellutla, S.; Stowe, A. C.; Dalal, N. S.; van Tol, J.; Bassil, B. S. *Inorg. Chem.* **2004**, *43*, 144–154.
(12) Mbomekalle, I. M.; Keita, B.; Nierlich, M.; Kortz, U.; Berthet, P.; Nadjo, L. *Inorg. Chem.* **2003**, *42*, 5143–5152.
(13) Fukaya, K.; Yamase, T. *Bull. Chem. Soc. Jpn.* **2007**, *80*, 178–182.
(14) Wassermann, K.; Dickman, M. H.; Pope, M. T. *Angew. Chem., Int. Ed.* **1997**, *36*, 1445–1448.
(15) Kortz, U.; Savelieff, M. G.; Bassil, B. S.; Dickman, M. H. *Angew. Chem., Int. Ed.* **2001**, *40*, 3384–3386.
(16) Fukaya, K.; Yamase, T. *Angew. Chem., Int. Ed.* **2003**, *42*, 654–658.
(17) Chen, L.; Zhao, J.; Ma, P.; Han, Q.; Wang, J.; Niu, J. *Inorg. Chem. Commun.* **2010**, *13*, 50–53.
(18) Fukushima, H. F.; Kobayashi, A.; Sasaki, Y. *Acta Crystallogr. Sect. B-Struct. Sci.* **1981**, *37*, 1613–1615.
(19) Müller, A.; Krickemeyer, E.; Dillinger, S.; Meyer, J.; Bögge, H.; Stammler, A. *Angew. Chem., Int. Ed. Engl.* **1996**, *35*, 171–173.
(20) Gaunt, A. J.; May, I.; Sarsfield, M. J.; Collison, D.; Helliwell, M.; Denniss, I. S. *Dalton Trans.* **2003**, 2767–2771.
(21) (a) Yang, Y.; Xu, L.; Gao, G.; Li, F.; Qiu, Y.; Qu, X.; Liu, H. *Eur. J. Inorg. Chem.* **2007**, 2500–2505. (b) Yang, Y. Y.; Xu, L.; Gao, G. G.; Li, F. Y.; Qu, X. S.; Guo, W. H. *J. Mol. Struct.* **2008**, *886*, 85–89.
(22) Li, L.; Shen, Q.; Xue, G.; Xu, H.; Hu, H.; Fu, F.; Wang, J. *Dalton Trans.* **2008**, 5698–5700.
(23) Xu, H.; Li, L.; Liu, B.; Xue, G.; Hu, H.; Fu, F.; Wang, J. *Inorg. Chem.* **2009**, *48*, 10275–10280.
(24) Li, S. Z.; Zhao, J. W.; Ma, P. T.; Du, J.; Niu, J. Y.; Wang, J. P. *Inorg. Chem.* **2009**, *48*, 9819–9830.
(25) Fidalgo, E. G.; Neels, A.; Stoeckli-Evans, H.; Süss-Fink, G. *Polyhedron* **2002**, *21*, 1921–1928.
(26) Sheldrick, G. M. *SHELXTL97, Program for Crystal Structure Solution*; University of Göttingen: Göttingen, Germany, 1997.
(27) Wu, Q.; Han, Q.; Chen, L.; Ma, P.; Niu, J. *Z. Naturforsch.* **2010**, *65b*, 163–167.
(28) Zhao, J. W.; Jia, H. P.; Zhang, J.; Zheng, S. T.; Yang, G. Y. *Chem.—Eur. J.* **2007**, *13*, 10030–10045.
(29) Li, L.; Liu, B.; Xue, G.; Hu, H.; Fu, F.; Wang, J. *Cryst. Growth Des.* **2009**, *9*, 5209–5212.
(30) Brown, I. D.; Altermatt, D. *Acta Crystallogr. Sect. B* **1985**, *41*, 244–247.
(31) He, Q.; Wang, E.; You, W.; Hu, C. *J. Mol. Struct.* **1999**, *508*, 217–221.
(32) Belai, N.; Pope, M. T. *Chem. Commun.* **2005**, 5760–5762.
(33) Wang, J. P.; Ma, P. T.; Li, J.; Niu, H. Y.; Niu, J. Y. *Chem. Asian J.* **2008**, *3*, 822–833.
(34) (a) Zheng, S. T.; Wang, M. H.; Yang, G. Y. *Chem. Asian J.* **2007**, *2*, 1380–1387. (b) Zhao, J. W.; Li, B.; Zheng, S. T.; Yang, G. Y. *Cryst. Growth Des.* **2007**, *7*, 2658–2664.
(35) Zhang, Z.; Liu, J.; Wang, E.; Qin, C.; Li, Y.; Qi, Y.; Wang, X. *Dalton Trans.* **2008**, 463–468.

(36) Dolbecq, A.; Compain, J. D.; Mialane, P.; Marrot, J.; Rivière, E.; Sécheresse, F. *Inorg. Chem.* **2008**, *47*, 3371–3378.
(37) Wang, J. P.; Du, J.; Niu, J. Y. *CrystEngComm* **2008**, *10*, 972–974.
(38) (a) Zheng, S. T.; Yuan, D. Q.; Zhang, J.; Yang, G. Y. *Inorg. Chem.* **2007**, *46*, 4569–4574. (b) Zhao, J. W.; Zheng, S. T.; Li, Z. H.; Yang, G. Y. *Dalton Trans.* **2009**, 1300–1306.
(39) (a) Zhao, J. W.; Zheng, S. T.; Yang, G. Y. *Chem. Commun.* **2008**, 570–572. (b) Zhao, J. W.; Jia, H. P.; Zhang, J.; Zheng, S. T.; Yang, G. Y. *Chem.—Eur. J.* **2008**, *14*, 9223–9229.
(40) (a) Wang, J. P.; Ma, P. T.; Li, J.; Niu, J. Y. *Chem. Lett.* **2006**, *35*, 994–995. (b) Wang, J. P.; Du, X. D.; Niu, J. Y. *Chem. Lett.* **2006**, *35*, 1408–1409.
(41) Li, B.; Zhao, J. W.; Zheng, S. T.; Yang, G. Y. *Inorg. Chem.* **2009**, *48*, 8294–8303.
(42) Kohler, A.; Gruner, J.; Friend, R. H.; Mullen, K.; Scherf, U. *Chem. Phys. Lett.* **1995**, *243*, 456–461.
(43) Wang, D. J.; Zhang, J.; Shi, T. S.; Wang, B. H.; Cao, X. Z.; Li, T. J. *J. Photochem. Photobiol. A* **1996**, *93*, 21–25.
(44) Kronik, L.; Shapira, Y. *Surf. Sci. Rep.* **1999**, *37*, 1–206.
(45) Qi, M. H.; Liu, G. F. *J. Phys. Chem. B* **2003**, *107*, 7640–7646.
(46) Lin, Y. H.; Wang, D. J.; Zhao, Q. D.; Li, Z. H.; Ma, Y. D.; Yang, M. *Nanotechnology* **2006**, *17*, 2110–2115.
(47) Dijken, A. V.; Meulenkamp, E. A.; Vanmaekelbergh, D.; Meijerink, A. *J. Phys. Chem. B* **2000**, *104*, 4355–4360.
(48) Lin, Y. H.; Wang, D. J.; Zhao, Q. D.; Yang, M.; Zhang, Q. L. *J. Phys. Chem. B* **2004**, *108*, 3202–3206.